JGR Space Physics

RESEARCH ARTICLE
10.1029/2024JA033082

Auroral Energy Deposition and Conductance During the 2013 St. Patrick's Day Storm: Meso-Scale Contributions

Christine Gabrielse[1], Y. Nishimura[2], J. H. Hecht[1], M. W. Chen[1], S. R. Kaeppler[3], D. M. Gillies[4,5], Y. Deng[6], E. Spanswick[4], E. Donovan[4], J. S. Evans[7], and L. R. Lyons[8]

[1]Space Sciences Department, The Aerospace Corporation, El Segundo, CA, USA, [2]Department of Electrical and Computer Engineering, Boston University, Boston, MA, USA, [3]Department of Physics and Astronomy, Clemson University, Clemson, SC, USA, [4]Department of Physics and Astronomy, University of Calgary, Calgary, AB, USA, [5]Department of Chemistry and Physics, Mount Royal University, Calgary, AB, USA, [6]Department of Physics, University of Texas at Arlington, Arlington, TX, USA, [7]Computational Physics, Inc, Springfield, VA, USA, [8]Department of Atmospheric and Oceanic Sciences, UCLA, Los Angeles, CA, USA

Key Points:

- Precipitation trends are investigated: meso-scales are important throughout the storm SSC and main phase albeit related to SML not SYM-H
- Median conductance is largest post-midnight during SSC but larger localized conductance peaks exist in pre-midnight sector throughout event
- We developed an all-sky-imager moonlight removal algorithm, allowing for better conductance, energy flux, and mean energy determination

Supporting Information:

Supporting Information may be found in the online version of this article.

Correspondence to:

C. Gabrielse,
christine.gabrielse@aero.org

Citation:

Gabrielse, C., Nishimura, Y., Hecht, J. H., Chen, M. W., Kaeppler, S. R., Gillies, D. M., et al. (2025). Auroral energy deposition and conductance during the 2013 St. Patrick's Day Storm: Meso-scale contributions. *Journal of Geophysical Research: Space Physics*, *130*, e2024JA033082. https://doi.org/10.1029/2024JA033082

Received 24 JUL 2024
Accepted 31 JAN 2025

Author Contributions:

Conceptualization: Christine Gabrielse, Y. Nishimura
Data curation: Christine Gabrielse
Formal analysis: Christine Gabrielse, Y. Nishimura, J. H. Hecht, M. W. Chen, S. R. Kaeppler, D. M. Gillies
Funding acquisition: Christine Gabrielse, Y. Deng
Investigation: Christine Gabrielse
Methodology: Christine Gabrielse, Y. Nishimura, S. R. Kaeppler
Project administration: Christine Gabrielse

Abstract Geomagnetic storms transfer massive amounts of energy from the sun to geospace. Some of that energy is dissipated in the ionosphere as energetic particles precipitate and transfer their energy to the atmosphere, creating the aurora. We used the Time History of Events and Macroscale Interactions during Substorms (THEMIS) mosaic of all-sky-imagers across Canada and Alaska to measure the amount of energy flux deposited into the ionosphere via auroral precipitation during the 2013 March 17 storm. We determined the time-dependent percent of the total energy flux that is contributed by meso-scale (<500 km wide) auroral features, discovering they contribute up to 80% during the sudden storm commencement (SSC) and >~40% throughout the main phase, indicating meso-scale dynamics are important aspects of a geomagnetic storm. We found that average conductance was higher north of 65° until SYM-H reached −40 nT. We also found that the median conductance was higher in the post-midnight sector during the SSC, though localized conductance peaks (sometimes >75 mho) were much higher in the pre-midnight sector throughout. We related the post-midnight/pre-dawn conductance to other recent findings regarding meso-scale dynamics in the literature. We found sharp conductance peaks and gradients in both time and space related to meso-scale aurora. Data processing included a new moonlight removal algorithm and cross-instrument calibration with a meridian scanning photometer and a standard photometer. We compared ASI results to Poker Flat Incoherent Scatter Radar (PFISR) observations, finding energy flux, mean energy, and Hall conductance were highly correlated, moderately correlated, and highly correlated, respectively.

Plain Language Summary Geomagnetic storms transfer massive amounts of energy from the sun to geospace—some of which is converted into the multi-colored aurora. Knowing how much energy enters Earth's upper atmosphere helps scientists better understand how Earth reacts to space weather events. The aurora's colors tell us how much energy is being deposited into Earth's atmosphere via energetic particles, which rain down from space and create light as they strike the atmosphere. Less energetic particles create red aurora, more energetic particles create green and blue aurora. We use cameras to measure the aurora's colors and determine the amount of energy entering the system related to smaller, often brighter and more dynamic aurora, in contrast to the more widely studied large-scale aurora. We discovered <500 km wide aurora contribute >40% of the energy entering the system over time throughout the main phase of the storm—sometimes up to 80%! This shows how important the smaller aurora are. The aurora makes the atmosphere more conductive, allowing it to connect more easily to outer space. Sharp changes in conductance allow electrical currents to flow. Our study found when and where conductance peaked during the storm and found sharp changes related to the <500 km aurora.

1. Introduction

Geomagnetic storms transport large amounts of energy between the sun, the magnetosphere, and the ionosphere-thermosphere. Because storms occur on global scales, energy transport is often considered on global scales. However, as our instrumentation improves to include higher spatial and temporal resolution, the importance of characterizing and understanding phenomena that occur on smaller, meso-scales (~10s-500 km in the ionosphere) has emerged. Are the larger, global scale aurora and related phenomena truly the most important contributors to

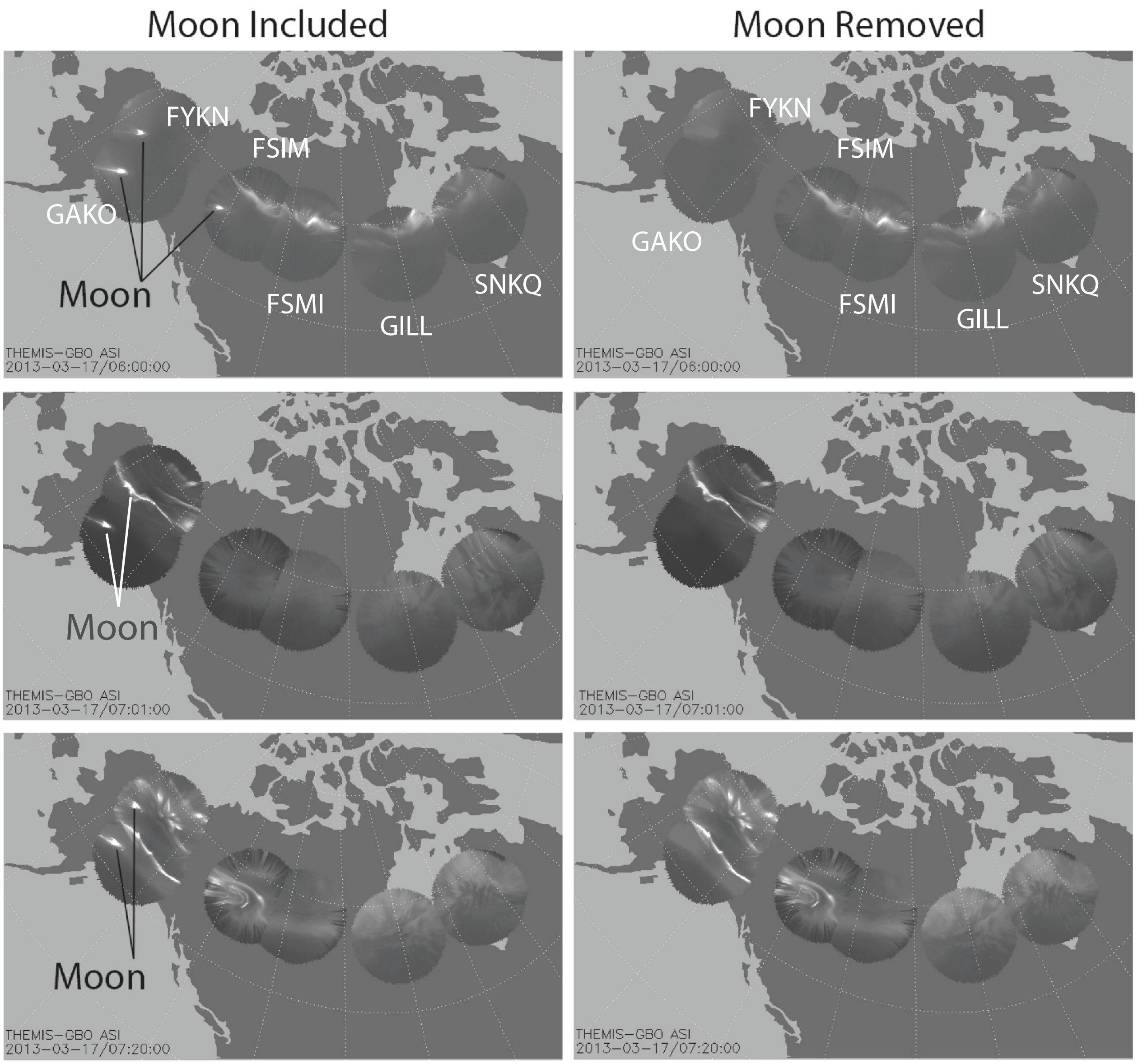

8 - F 1)) 8 / F 1)) 8 / 7%F77 3
8 4 7(F7 3 8 4 7(F 7 32 8 4 P / 3I F 2 8
; @I A , 3 8 48 6 2 8 6 /4) 2 8 / 8
3 2 2 4 8 8 2 8 8 2 6 6 6
8 /

2 8 2 &3 6 / C C4 8
2 3. 2 / 7 4? 2 8 8
2 /) & 8 2 6 2 8
2 8 &) &/
2 8) – – 3 4
) 8 /
C/ 9 8 M % /%9 /79 / 1 8 8
8 & / 2
2 8 8 8 8 2 / 8 1
/ 3 77 4 8 2 8 &

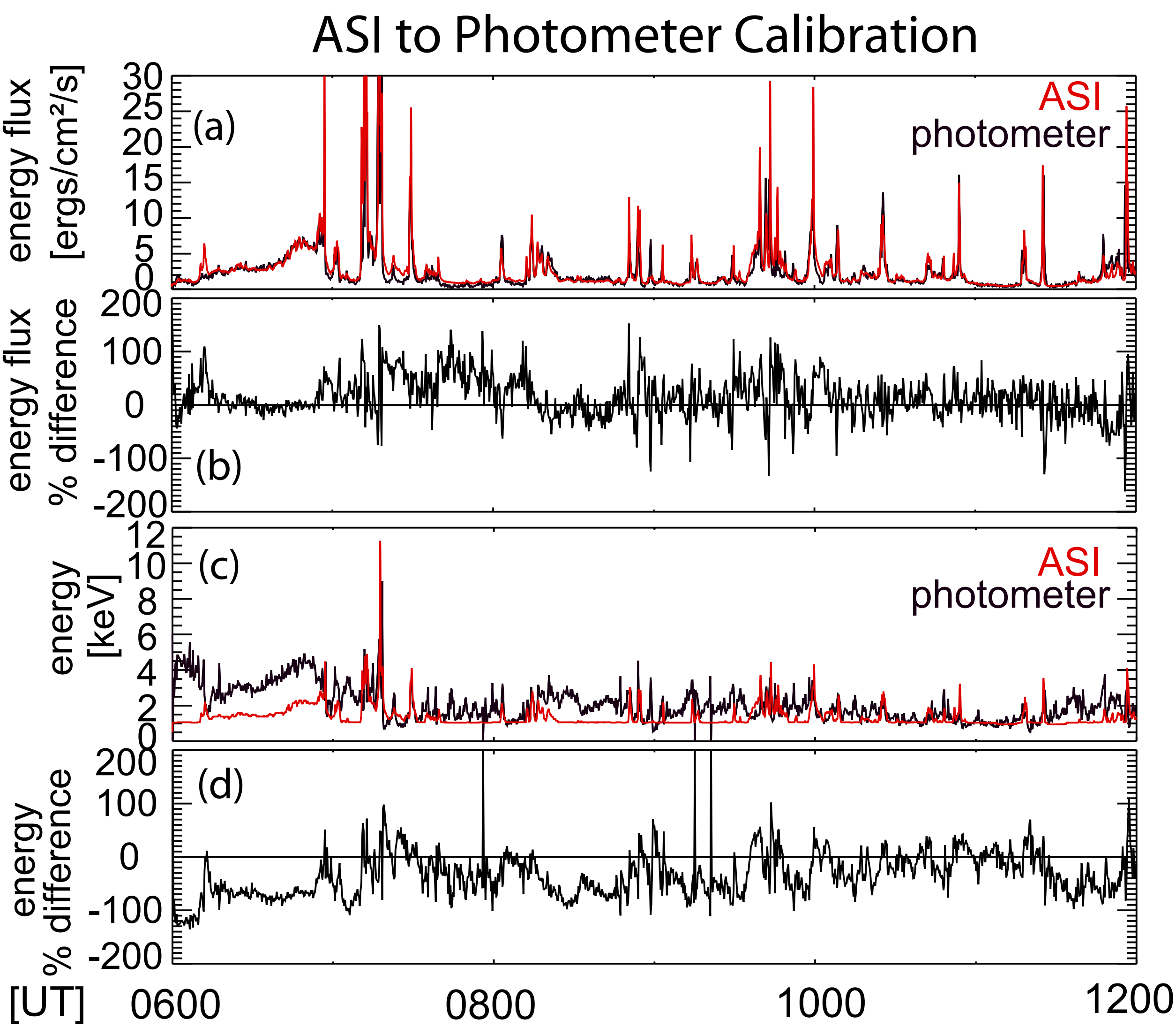

8 3 4 & 2 ; 6 2) 3 4 32 64/ 324 2 8)
&/ 3 4 2 2) 3 4 32 64/ 3 4 2 8) /

8 2 / 8 8 6 8
/

- 6 8) 5 6 8 8 8
8) 2 / 0 8 2
8 2 8) / &
2 8 6 ; 6 2 2 /
2 8
2 8 2 2 8 /

2 8 6) 2 2
8 2 & P 3 / 4/
8 38 4
8 6 / & 8 2
2 3 1 / 7 4/ A &
/

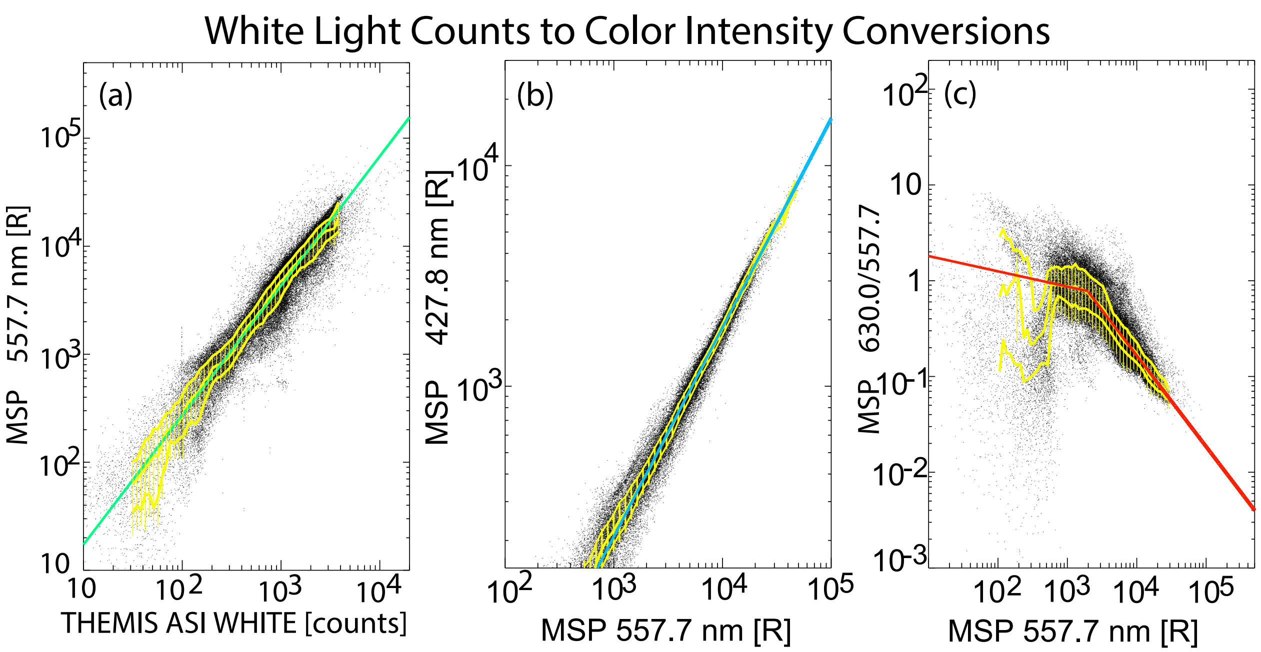

8 3 4 ! (/(1)) 8 /; 8 8 M 8 M /
8 6 2 /. /324 3 4 2 ! 5 2 (/ (/(/3 4
3 4 2 ! 5 2 % 7/7 (/(/(/ 8 8 8 2 8 (/(% 7/7 (/(
8 (/(M /

2 4 0 8

2 & 8 8
. 2 /3 7 4 8) 3 (/(4 2 3 (/ 4
3% 7/7 4 / 8 8
2 / 0 !
8) 2 G
3 4/ 30
2 2 /40 7 2
5 32 8 7 777 7 P 7 2 % 7 P
7 4/ 8 5
5 /) 7 8
8 L % 7 7 7 P 7 / 0
% 7 2 2 8
2 8 M /

8 F

. ((7 7 7 C C 7 8

(8 7 7 7 7 C (7

% 7 7 8 7 7 7 7 C 7

% 7 7 8 7 7 7 (7 C 7

5 3) 2 / CC7 4 5 8 F

M F%/ 7 (/ 7
M F / 7 (/ 7

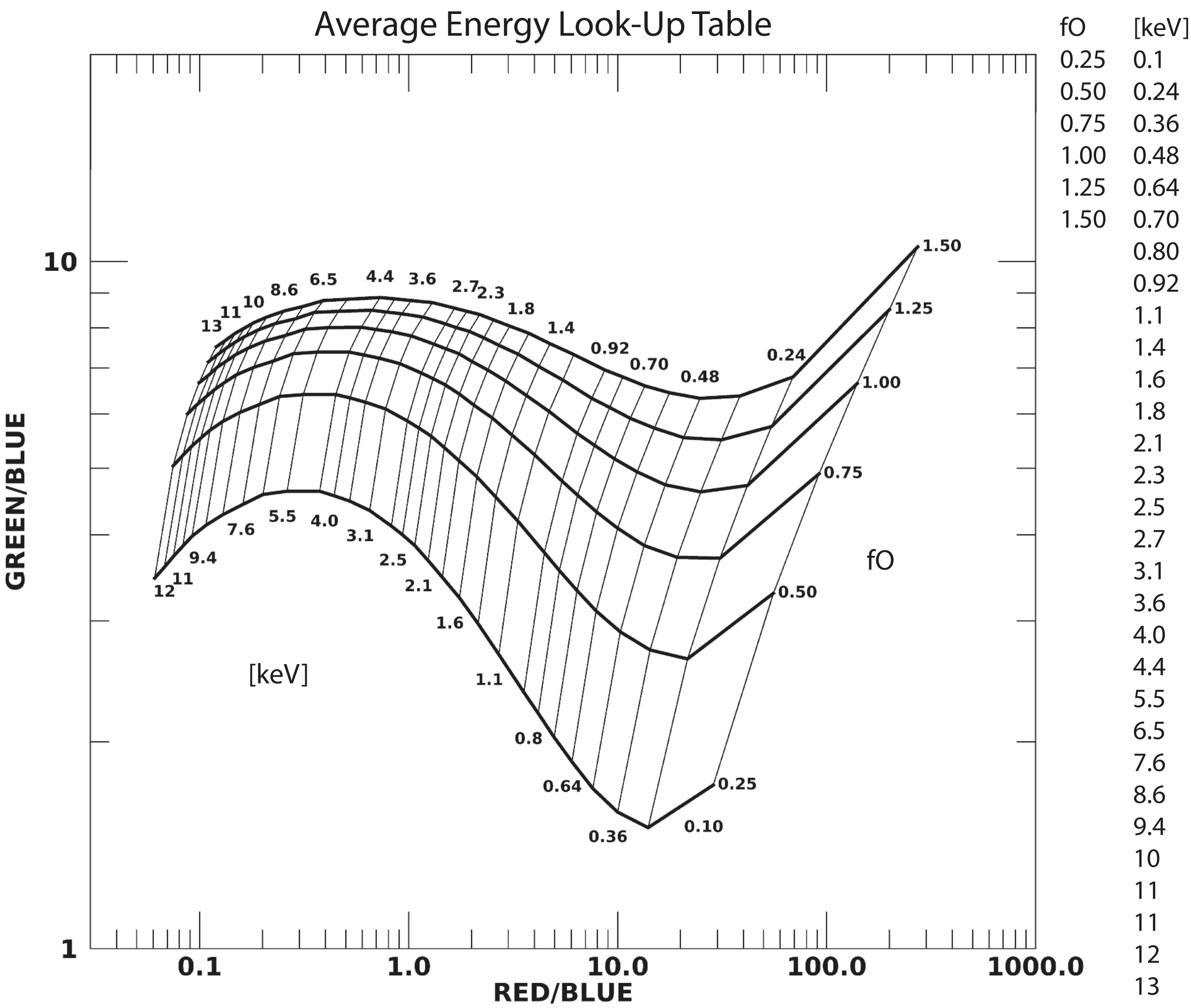

8 , 65 2 7 7 / 5 & 2 5 & 2 /
, 6 / 8 ,
/ I 2 8 8 8 8 2 6 /

2 7 (/ 0 37/ 7 7/ ((7/C /(C / / %/(6 4
& 3 7 77 /4 2 65 2 1
/ 0 2 8
& & /

8 8 2 / 3 C (4 8
1 W 2 F

W 7 % -

W W 7 −7 %

8 W ! &/

0 1 !) 8 2 . 2 / 3 7 4
M 7 N 3 C% 4F

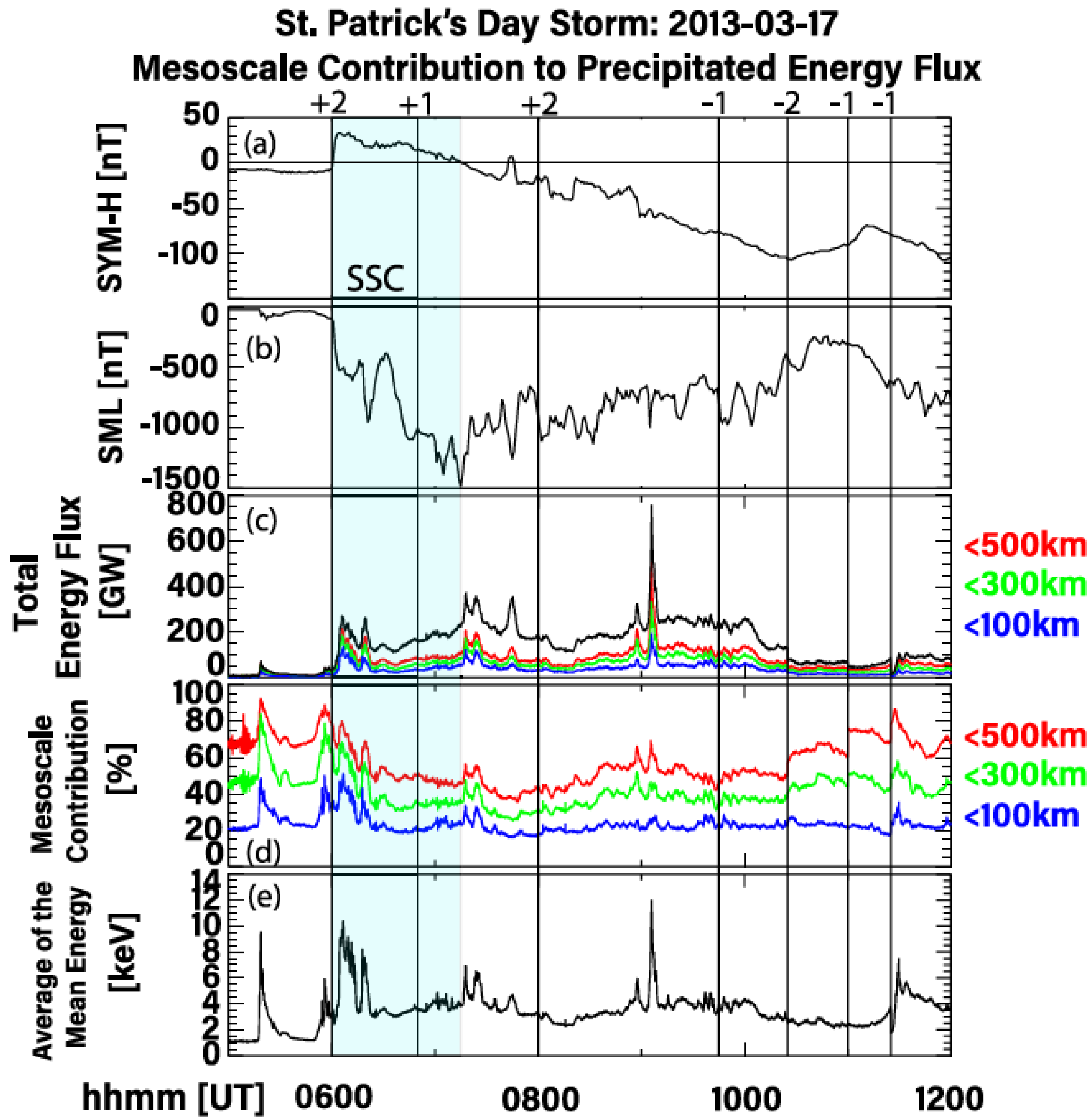

Figure 5. (a) SYM-H. (b) SML index. (c) Total energy flux (power) observed by the THEMIS ASIs. (d) The percent contribution to the power from meso-scale auroral forms with scale sizes <500 km (red), <300 km (green), <100 km (blue). (e) The average of the mean energy observed by the THEMIS ASIs. Vertical lines mark when ASI stations turned on or off. The numbers at the top indicate the number of stations turning on (e.g., +2 means two stations turned on) or off (e.g., −1 means one station turned off). For most stations this was when the sun set (on) or rose (off), though some stations we kept off when the moon was up and there was no aurora.

shortly after the quick SYM-H and SML index decrease, at 09:06 UT (~12 keV). Finally, we also pointed out a lesser peak in energy flux and mean energy at 08:19:16 UT, which corresponds with another SML index peak and an increase in SYM-H.

In addition to plotting the total energy flux (power), we separated the contributions of three different meso-scales to the total: <500 km, <300 km, and <100 km, in Figure 5d. We used the same 2D median filter method in Gabrielse et al. (2021) to determine the contributions. For example, to determine the amount of power contributed by scale sizes 500 km and less, we found the median across 500 km in 2D (both latitude and longitude directions)

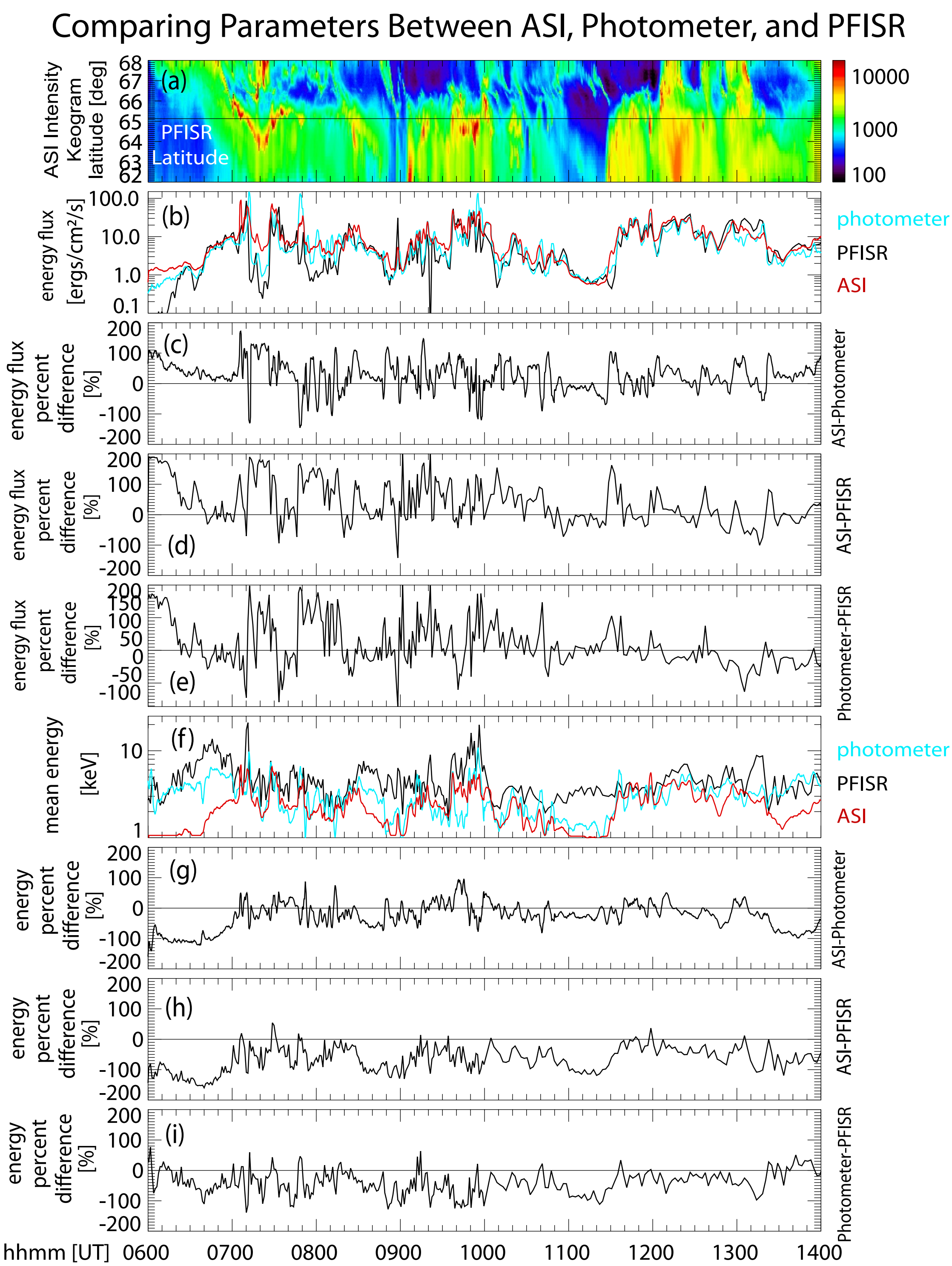

8 . 3 4@ 8 !) /324 & 2 ! 6 2 32 4) 32 64)3 4/3 4! 2 8) & 2 /3 4! 2 8) !) & 2 /3 4! 2 8 !) & 2 /34 2 ! 6 2 32 4) 32 64)3 4/3 4! 2 8) 2 /3 4! 2 8) !) 2 /34! 2 8 !) 2 /

Table 1
Percent Differences Between ASI, Photometer, and PFISR Data

ASI versus photometer versus PFISR percent difference 06–14 UT	Mean	Median	Lower quartile	Upper quartile	Correlation Coefficient
ASI versus Photometer Q	26.2	25.7	14.6	38.4	0.6
ASI versus Photometer $\overline{E}$	−26.5	−23.2	−33.3	−12.2	0.5
ASI versus PFISR Q	44.9	28.7	7.5	65.3	0.7
ASI versus PFISR $\overline{E}$	−67.5	−70.4	−83.3	−50.1	0.4
Photometer versus PFISR Q	20.5	0.5	−15.4	23.0	0.3
Photometer versus PFISR $\overline{E}$	−41.5	−42.1	−53.7	−28.4	0.5
ASI versus photometer versus PFISR percent difference 10–14 UT	**Mean**	**Median**	**Lower quartile**	**Upper quartile**	**Correlation Coefficient**
ASI versus Photometer Q	18.4	18.2	4.9	28.3	0.9
ASI versus Photometer $\overline{E}$	−22.0	−20.7	−27.9	−13.5	0.6
ASI versus PFISR Q	10.0	−1.5	−10.0	18.4	0.8
ASI versus PFISR $\overline{E}$	−55.7	−51.7	−70.4	−44.3	0.5
Photometer versus PFISR Q	−6.8	−13.1	−23.6	−0.6	0.8
Photometer versus PFISR $\overline{E}$	−34.2	−33.0	−43.8	−24.1	0.5

on average underestimates the mean energy by ~20%. This is improved from the ASI-Photometer comparison at Fort Yukon (Figure 1), for which the ASI underestimated the mean energy by ~49%. Because the ASI and photometer were both looking up the same direction in Figure 1, this indicates that the elevation angle may not be the biggest culprit in mean energy uncertainty.

Regarding the difference from 11:00 to 11:30 UT, the PFISR average energy remains fairly constant whereas there is a significant decrease in the average energy from the optical techniques. The PFISR observations showed a consistent electron density during this interval of time; the average energy was estimated using the maximum entropy method technique (see Section 2.3). Near 13:00 to 13:30 UT, there was an increase in the average energy from the PFISR observations relative to the imager methods. During this time, the maximum entropy method showed good agreement between modeled and observed densities above 100 km altitude, but there was a peak in the modeled electron density that did not match the PFISR observations below 90 km altitude. This likely contributed to PFISR's increase in mean energy. Further investigation is required to understand how to more effectively model this interval, but that is outside of the scope of the current investigation. In general, the PFISR maximum entropy method performed well in producing modeled electron density profiles that were consistent with the observations.

The mean energy underestimation by the optical instruments in comparison to the PFISR results contrasts with the energy flux comparison, which had an average percent difference of only 10% with a median percent difference of −1.5% and a correlation coefficient of 0.8. Although differences are expected when using different instruments that use different techniques and assumptions, we are unsure of the exact source of the median −33% difference between the photometer and PFISR mean energies, since they are co-located and both looking up a very similar direction. It seems unlikely that a difference of 33% would arise from the fact that PFISR looks straight up zenith whereas the photometer looks up the magnetic field line. Because it is difficult to know which is correct, we report percent difference rather than percent error.

The better match between datasets for energy flux makes sense, because the energy flux is almost entirely a function of the blue line emission, which is almost entirely a function of the green line emission, which is well-correlated to the white light (Figure 3). A future work is to include redline imagers from the Canadian Space Agency's Geospace Observatory Canada initiative, as well as to use calibrated RGB cameras from the University of Calgary's TREx array. The addition of a redline imager will improve the mean energy estimate for the ASI method, and we expect ASI results to then better match the photometer's.

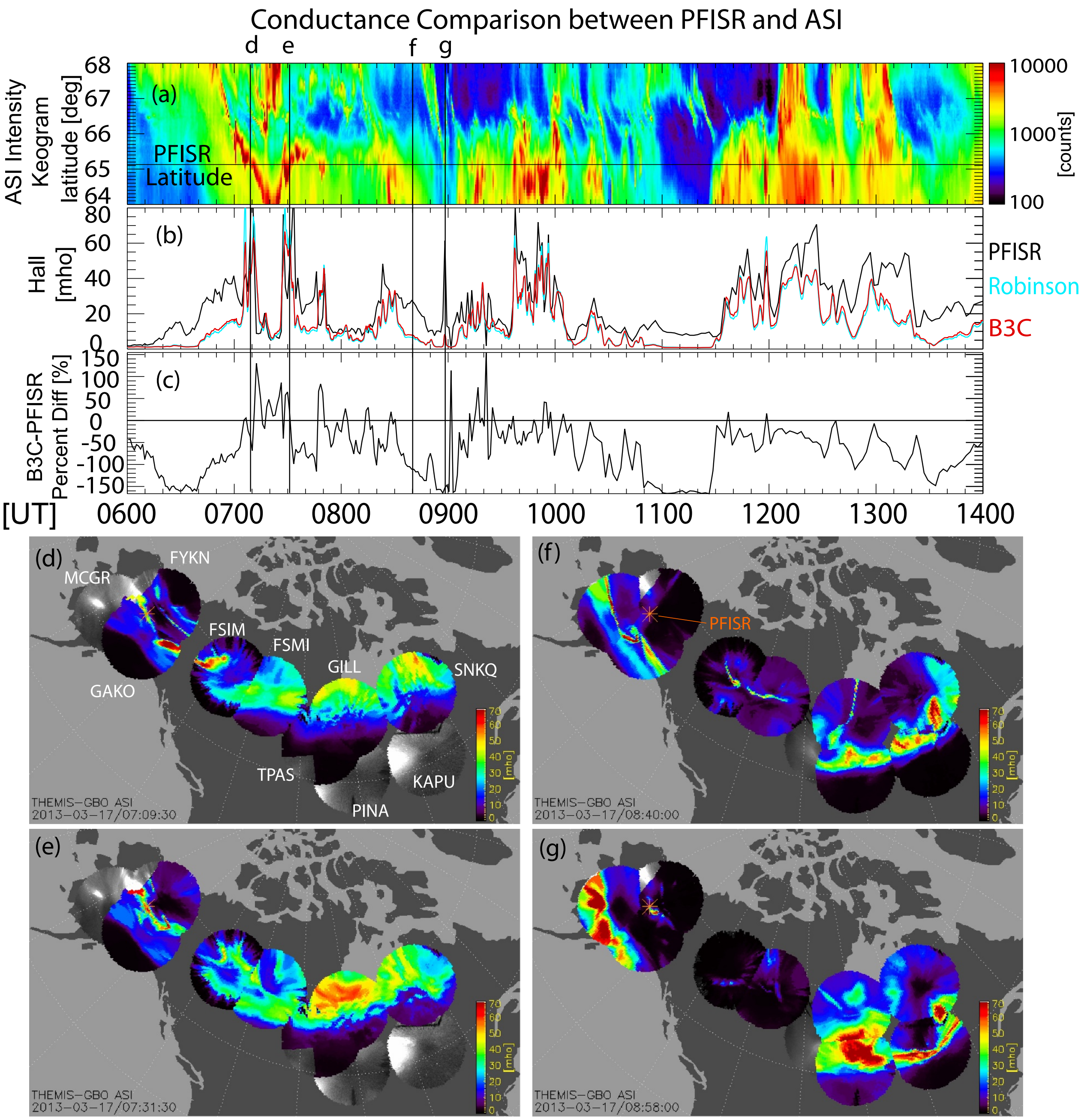

8 1 3 4@ 8 !) / !) 8 /3 2 4
1 2 !) 32 64 ; 6) !) 3 4 2 32 4
) & /3 4 2 8 5 1 !) 5 1 /3 4P
3 4 1) 8 / 2 3 4/ !) A 6 8 6/
8 3 4 8 & 3 4
F 8 8 5 8 &
. 7(F7 7 F7 8 . @, 2 . 8 . 8 2
2 & 6 /

- 77 2 8
- / (
8 - ; 51 M
/ 8) 2
2 (/ 2 C7

10.1029/2024JA033082

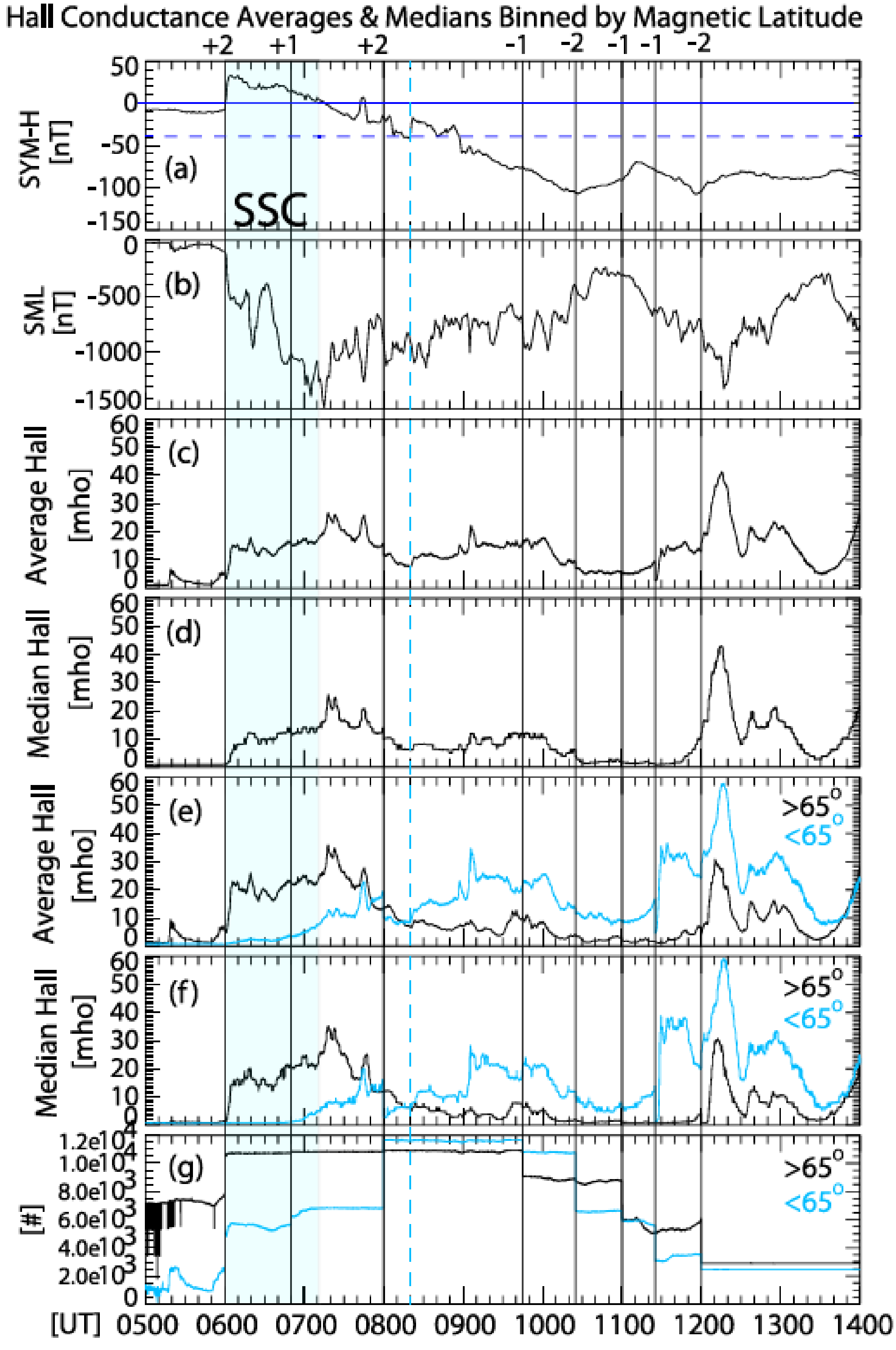

Figure 8. (a) SYM-H. Solid horizontal line drawn at 0 nT. Dashed horizontal line drawn at −40 nT. (b) SML. (c) Average and (d) Median Hall conductance over all gridded data where precipitation occurred. (e) Average and (f) Median Hall conductance over all gridded data where precipitation occurred north of 65° magnetic latitude (black) and south of 65° magnetic latitude (blue). (g) The number of data points used to calculate (e) and (f) north of 65° magnetic latitude (black) and south of 65° magnetic latitude (blue). Solid black vertical lines mark when additional ASIs were added or subtracted from the dataset. The number of ASIs added or subtracted is marked with, for example, +2, above panel (a). The blue dashed vertical line marks when the average and median conductance grew larger in the southern hemisphere, which is when SYM-H first reached −40 nT. The sudden storm commencement (SSC) is colored in a transparent blue box.

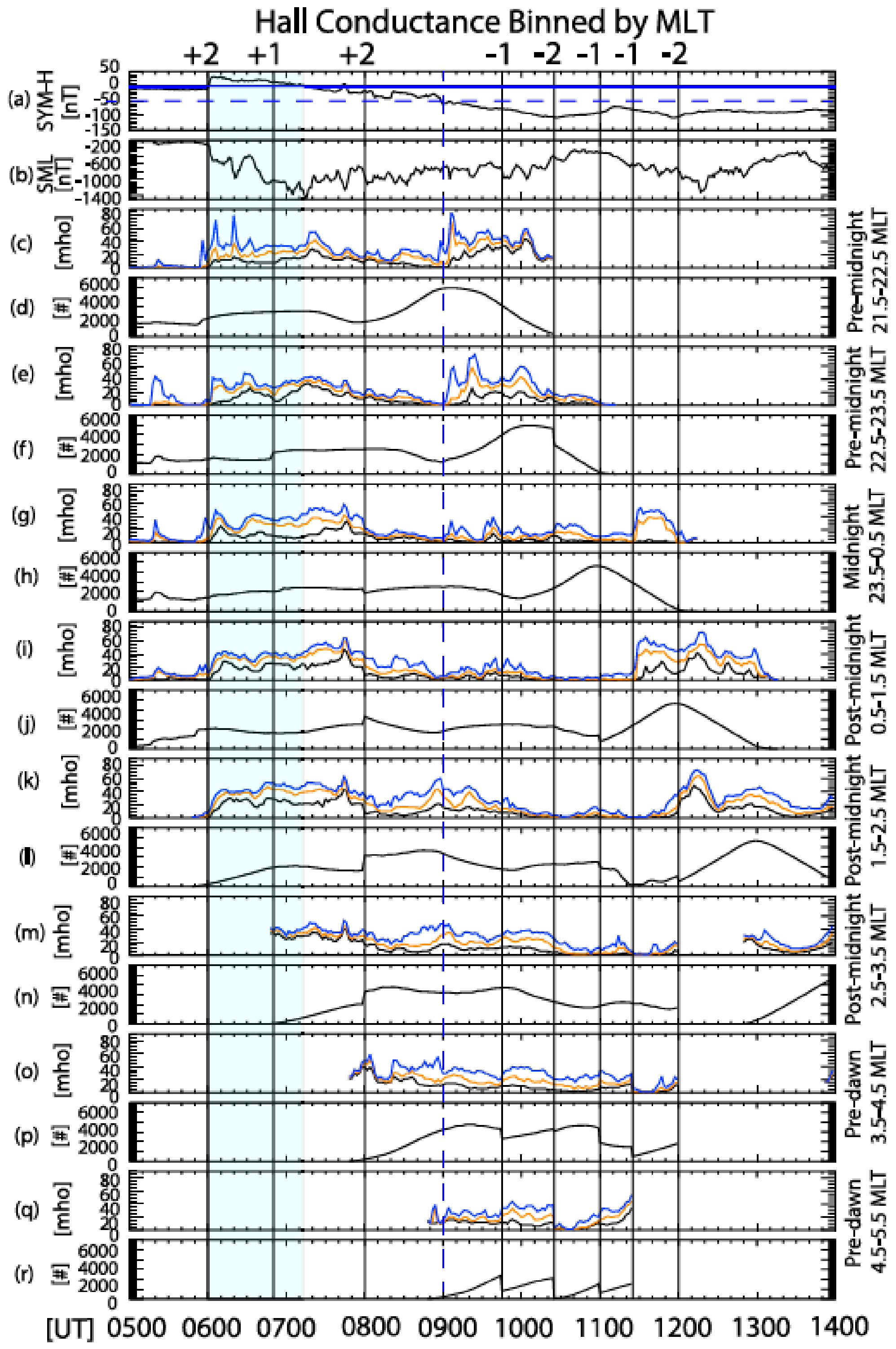

Figure 9. (a) SYM-H. Solid horizontal line drawn at 0 nT, dashed horizontal line drawn at −50 nT. (b) SML index. (c) The median and upper quartile of the Hall conductance from precipitation between 21.5 and 22.5 MLT. (d) The number of data points used to determine (c). (e) The same as (c) but within 22.5–23.5 MLT. (f) The number of data points used to determine (e). (g) The same as (c) but within 23.5–0.5 MLT (midnight). (h) The number of data points used to determine (g). (i) The same as (c) but within 0.5–1.5 MLT. (j) The number of data points used to determine (i). (k) The same as (c) but within 1.5–2.5 MLT. (l) The number of data points used to determine (k). (m) The same as (c) but within 2.5–3.5 MLT. (n) The number of data points used to determine (m). (o) The same as (c) but within 3.5–4.5 MLT. (p) The number of data points used to determine (o). (q) The same as (c) but within 4.5–5.5 MLT. (r) The number of data points used to determine (q). Vertical lines mark when additional ASIs were added or subtracted from the dataset. The number of ASIs added or subtracted is marked on the top of the figure (e.g., +2). Dashed vertical line drawn at 09:00 UT when SYM-H reaches −50 nT. The sudden storm commencement (SSC) is colored in a transparent blue box.

Table 2
ASI Versus PFISR Hall Conductance Percent Difference 06–14 UT

	Mean	Median	Lower quartile	Upper quartile	Corr. Coeff.
B3C Hall	−63.6	−62.2	−108.1	−25.2	0.8
Robinson Hall	−68.6	−69.5	−114.5	−34.7	0.7
When ASI conductance > 1 mho					
B3C Hall	−59.4	−57.8	−98.5	−23.8	0.8
Robinson Hall	−65.9	−66.0	−109.7	−32.7	0.7
When ASI conductance > 5 mho					
B3C Hall	−40.2	−44.5	−75.4	−13.3	0.7
Robinson Hall	−47.1	−51.9	−84.4	−21.2	0.7
When ASI conductance > 10 mho					
B3C Hall	−31.7	−38.3	−67.4	−8.2	0.6
Robinson Hall	−36	−42.5	−73	−13	0.6

percentile. Around 09:00 UT, we see a large activation of the aurora with localized increases in precipitation, energy flux, and Hall conductance, which show up in the 1.5–2.5 MLT sector and both pre-midnight sectors' 75th and 90th percentile plots. We do not see a huge associated increase in SML. The conductance falls off in the pre-midnight sector by 11:00 UT, which is when we lose coverage of the pre-midnight sector due to Earth's rotation. At 11:25 UT, the conductance increases in the midnight and post-midnight sectors, with localized conductance (75th and 90th percentiles) much higher than broader (median) conductance near midnight.

On meso-scales, we note that conductance has large variability—something we see demonstrably in Figure 7. There are 10s of mho spatial and temporal gradients throughout the event, each lasting only several minutes at a fixed location (see Movie S3 of the conductance evolution). Their temporal variability is captured by the 90th percentile plots in Figure 9. Often, the 90th percentile peaks last on the order of 10 min. We see the temporal gradients highlighted in Figure 7b and the spatial gradients highlighted in Figures 7d–7h. Sharp spatial gradients such as these are important to field-aligned current generation and may be related to stronger field-aligned currents that couple the magnetosphere to the ionosphere (Boström, 1974).

4.4. Uncertainties: Comparing Conductance From ASIs With PFISR

Similar to Section 4.2, we investigate conductance uncertainties by comparing values from the nearest ASI grid pixel to PFISR in Figure 7. Of course, both instruments have their own uncertainties and sources of error, which is why we calculate percent difference rather than percent error. Figure 7a is a keogram of white light intensity at the Poker Flat longitude, with a horizontal line drawn at the Poker Flat latitude. Figure 7b is a plot of the Hall conductance from PFISR (black), the B3C values using ASI inputs (red), and the Robinson formulae using the ASI inputs (blue). We smoothed the ASI-informed conductances to match the PFISR integration times, which varied over the hours long interval. The ASI and PFISR data follow similar trends, capturing large conductance increases from bright aurora and lower conductances when the aurora is dimmer. We included the percent difference between the ASI-informed B3C Hall conductance and the PFISR Hall conductance in Figure 8c. Table 2 includes the mean, median, and quartiles of the percent differences as well as the correlation coefficient between the conductances determined from ASI versus PFISR data.

Unlike Gabrielse et al. (2021), who found median percent differences of 18%–24% between ASI conductance and PFISR conductance, for this event we consistently measure lower Hall conductance from the ASI than from PFISR. The average and median percent differences are both in the −60% range for both B3C- and Robinson-determined conductance. This tracks with the fact that both the photometer and ASI consistently reported lower mean energies than PFISR. However, the correlation coefficient for both B3C and Robinson conductance, when compared to PFISR conductance, is 0.8, indicating correlation.

The percent error in the Hall conductance associated with uncertainties in the mean energy can be estimated using the Robinson equations given by 5 and 6. Robinson et al. (1987) used limits of integration of 500 eV to 30 keV

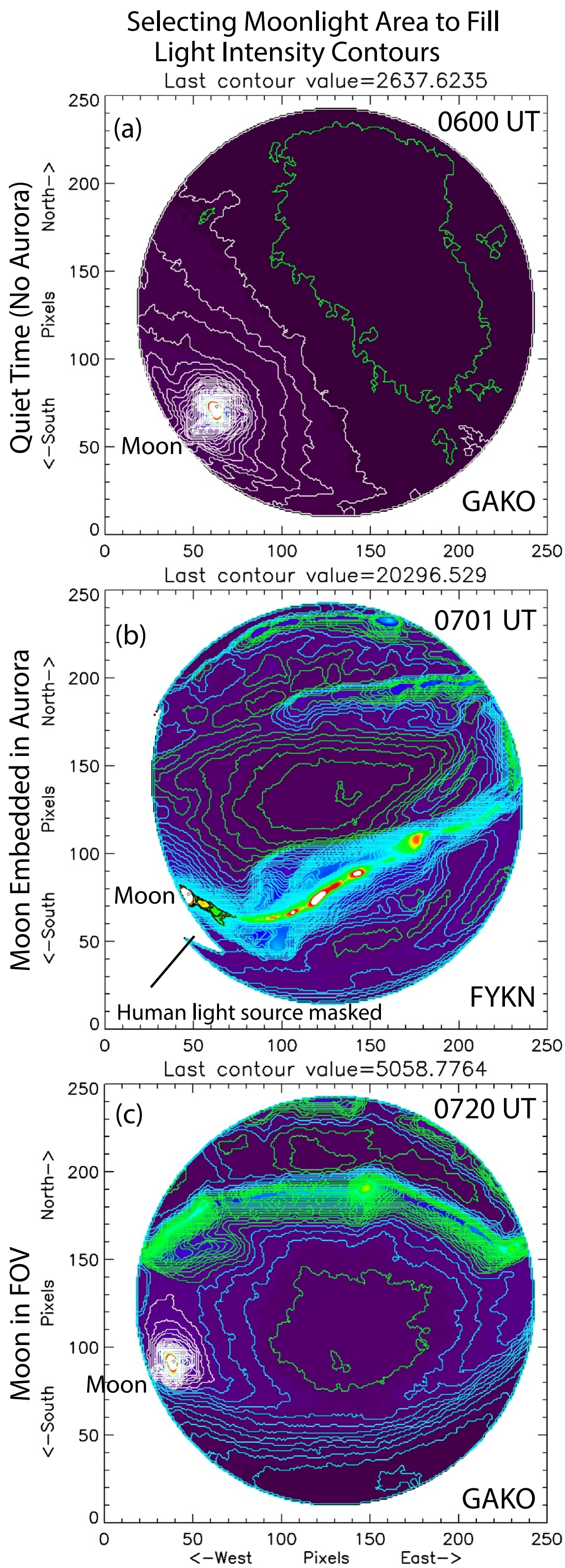

Selecting Moonlight Area to Fill
Light Intensity Contours
Last contour value=2637.6235
(a)
0600 UT
Moon
GAKO
Quiet Time (No Aurora)
<–South Pixels North–>
Last contour value=20296.529
(b)
0701 UT
Moon
Human light source masked
FYKN
Moon Embedded in Aurora
<–South Pixels North–>
Last contour value=5058.7764
(c)
0720 UT
Moon
GAKO
Moon in FOV
<–South Pixels North–>
<–West Pixels East–>

8